Research Article | Vol. 31, No. 7 / 27 Mar 2023 / Optics Express 11395
Optics EXPRESS

Spectral properties of intermediate to high refractive index nanocubes

TRISTAN MADELEINE,[1,*] GIAMPAOLO D'ALESSANDRO,[1] AND MALGOSIA KACZMAREK[2]

[1]Mathematical Sciences, University of Southampton, Southampton SO17 1BJ, United Kingdom
[2]Physics and Astronomy, University of Southampton, Southampton SO17 1BJ, United Kingdom
[*]tm3u18@soton.ac.uk

Abstract: Plasmonic resonances in sub-wavelength cavities, created by metallic nanocubes separated from a metallic surface by a dielectric gap, lead to strong light confinement and strong Purcell effect, with many applications in spectroscopy, enhanced light emission and optomechanics. However, the limited choice of metals, and the constraints on the sizes of the nanocubes, restrict the optical wavelength range of applications. We show that dielectric nanocubes made of intermediate to high refractive index materials exhibit similar but significantly blue shifted and enriched optical responses due to the interaction between gap plasmonic modes and internal modes. This result is explained, and the efficiency of dielectric nanocubes for light absorption and spontaneous emission is quantified by comparing the optical response and induced fluorescence enhancement of nanocubes made of barium titanate, tungsten trioxide, gallium phosphide, silicon, silver and rhodium.

1. Introduction

Metasurfaces made of metallic nanostructures, deposited on a dielectric coated metallic substrate, support strong plasmonic modes in the nanometer thin dielectric film [1]. A broad range of different nanostructures have already been investigated for their resonant optical response and, depending on their method of fabrication, they can be broadly classed into two categories: top-down systems fabricated through cleanroom techniques [2–4] and bottom-up self-assembly of nanoparticles [1,5–8]. An example of the latter are metal - insulator - metal (MIM) systems made of plasmonic nanostructures self-assembled on a nanometer thick dielectric coated metallic film, see Fig. 1. These offer particularly attractive configurations with an intense electromagnetic field confined to a nano-cavity under the nanostructures [9], thus forming an ideal setup for applications that rely on strong light-matter interaction and on the Purcell effect.

Such systems, often referred to as a nanopach antenna (NPA), have been theoretically [10] and experimentally studied, including some elegant configurations with fluorophores [11], dyes [9,12], PbS [13–15] and nanodiamonds [16] quantum dots, and semiconductors [17,18] incorporated in the gap under the nanostructures. More complex setups involving dimers of NPA have also been investigated for their additional modes excited in between the nanostructures [19,20]. NPA made of nanospheres and nanocubes are particularly interesting as they benefit from a natural polarization independent optical response [1,9].

The optical properties of NPAs strongly depend of the materials used, the dimension and shape of the nanocubes [21,22], as well as the thickness of the gap [7,23]. In this work we focus on nanocubes, a promising system that offers a greater potential for applications than nanospheres, due to their larger contact area with the dielectric subwalevength volume gap under the nanocubes. Materials combinations studied so far include, for example, gold [23] or silver [11] for substrates, a polyelectrolyte multilayer (PEM) for the gap to attach the nanocubes on

#485872 https://doi.org/10.1364/OE.485872
Journal © 2023 Received 18 Jan 2023; revised 19 Feb 2023; accepted 26 Feb 2023; published 20 Mar 2023

Optics EXPRESS

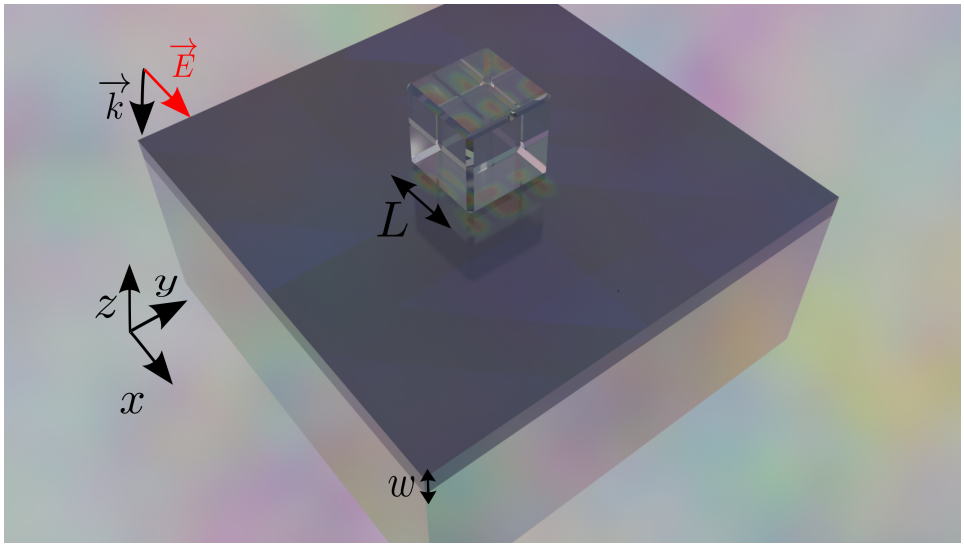

Fig. 1. Schematic diagram of the nano-patch antenna: a cube of size L is located on a dielectric film of thickness w coating a silver substrate. The coordinate axes, polarization of the incident light field E and direction of propagation normal to the substrate, $\vec{k}$, are indicated by the arrows. A typical gap mode of the system is represented for illustration purposes underneath the cube.

the surface [23], and silver [23], gold [24] or rhodium [25] nanocubes. Nanocubes found in the literature are typically between 50 nm and 150 nm wide and the gap is less than 20 nm thick. Such MIM configuration are an attractive platform due to the existence of the coupled surface plasmons at each dielectric-metal interface, resulting in an intense electromagnetic field confined in the nano-cavity under the cube, enabling the multiple applications for surface-enhanced Raman scattering [26], spectroscopy [27,28] and those cited above through intense light-matter interaction and Purcell effect. However, this configuration is limited by the cube sizes and materials available. These constrain the usable region of the optical spectrum, namely from the near-IR [14] (900 nm) to the blue [29] (500 nm), with the exception of small 59 nm rhodium nanocubes, with modes at the UV limit of the visible spectrum [25]. A potential way to overcome the MIM limitations, and to reduce the inherent losses via Joule's effect in the metals, is to consider configurations with non-metallic materials, as demonstrated through extensive research done on hybrid combinations of metals and dielectric [30–35] and all-dielectric metasurfaces of nanopillars and other shapes [36,37].

In this work, we focus on hybrid NPAs, formed by using combinations of dielectric and metals, such as dielectric nanospheres [38] and nanodisks [39] on a metal substrate. Here we focus on replacing the metallic nanocube with a dielectric one, i.e., we analyze the response of an insulator-insulator-metal (IIM) NPA. Such structure still enables the existence of resonant surface plasmons underneath the nanocube, hinting to similar applications of the MIM configuration. While different dielectric materials can, in principle, be used to support plasmons, it is important to consider current fabrication and experimental constraints. Hence, in this study, we only investigate the dielectrics for which the fabrication of stable nanocubes or parallelepipedal nanostructures has been successfully demonstrated, namely nanocubes made of Silicon [40] (Si), Gallium Phosphide [41] (GaP), barium titanate [42,43] (BTO) and tungsten trioxide WO_3 [44,45]. The latter is an electrochromic material, whose optical properties can be tuned by doping

Optics EXPRESS

with ions, either dynamically or at fabrication [46]. For simplicity, however, we consider pure WO_3 whose optical properties are well documented [46].

We numerically investigated, via COMSOL simulations, the optical properties of hybrid NPA made of BTO, WO_3, Si and GaP and compared them to Ag and Rh NPA. We also estimated the potential applications of these hybrid NPA for the applications mentioned above by computing the respective fluorescence of fluorophores deposited in the gap under the nanocube. The increase in fluorescence, enabled by the presence of the nanocubes is particularly interesting as it involves both enhanced light absorption, leading to intense localised electromagnetic fields, and enhanced spontaneous emission through the Purcell effect [11]. We saw that high refractive index (n>3) dielectric nanocubes and intermediate refractive index (1.9<n<3) dielectric nanocubes have distinct properties. Therefore, we analyze them separately. Intermediate refractive index hybrid NPA (BTO and WO_3) have similarly strong, but significantly blue-shifted plasmonic modes, with respect to their metallic counterparts. This results extends the previous studies exhibiting a shift in the wavelength of the applications of hybrid structures made of metallic nanoparticles on a dielectric substrate [47–50]. We explain this with a simple model based on the dispersion relation of the electromagnetic modes propagating in the gap. They also exhibit weak internal modes with little influence on the gap plasmonic modes. On the other hand, high refractive index hybrid NPA (Si and GaP) have strong hybridised internal and gap plasmonic modes leading to an enriched spectrum. We have not considered materials with smaller refractive indices because their mode confinement properties become weaker and weaker as the cube refractive index approaches that of the surrounding medium.

2. Results and discussion

2.1. Intermediate refractive index materials

We have numerically computed the mode structure of 150 nm wide nanocubes with an optically thick silver substrate coated by a 10 nm thick polyelectrolyte multilayer (PEM) illuminated at normal incidence, as described in the method section. We compared the optical response of nanocubes made with four different materials. We selected two metals, silver and rhodium, for comparison with the literature, silver being a benchmark material for strong gap plasmonic resonances [1] and rhodium for having resonant modes in the blue near-UV [25]. We start by only considering two intermediate refractive index dielectrics, WO_3 and BTO.

As can be seen in the upper part of Fig. 2, BTO and WO_3 exhibit sharp and deep resonances that are blue shifted as compared to silver. Indeed, the plasmonic modes of BTO and WO_3 nanocubes are respectively shifted by 150 nm, (mode a) at 410 nm, and 170 nm, (mode c) at 390 nm, compared to the same order plasmonic mode of silver nanocubes, (mode h) at 560 nm. We also see lower order modes for the BTO and WO_3 nanocubes at 520 nm, (mode b), and 480 nm, (mode d), while the corresponding mode for silver nanocubes is beyond the range of the spectrum plotted. Although the dielectric nanocubes have much sharper and deeper resonances than rhodium nanocubes, with the (mode f) barely detectable at 440 nm, silver nanocubes have strong higher order modes in this region, such as the (mode e) at 400 nm.

The existence of such sharp resonances opens the possibility of observing strong light-matter interaction underneath the dielectric nanocubes. In a generic NPA, two processes intervene to enhance the fluorescence: the strong enhancement of the electromagnetic field in the nanometer thick cavity significantly enhances the excitation of the fluorophores and the presence of the cavity enhances the spontaneous emission of light via the Purcell effect. To quantify this effect, we computed the fluorescence enhancement of fluorophores, such as sulfo-cy5 carboxylic acid deposited in the PEM material, between a configuration with and without nanocubes, following the procedure used in the literature [11,12]. The fluorophores are modelled by a dipolar moment $\boldsymbol{p}$.

Optics EXPRESS

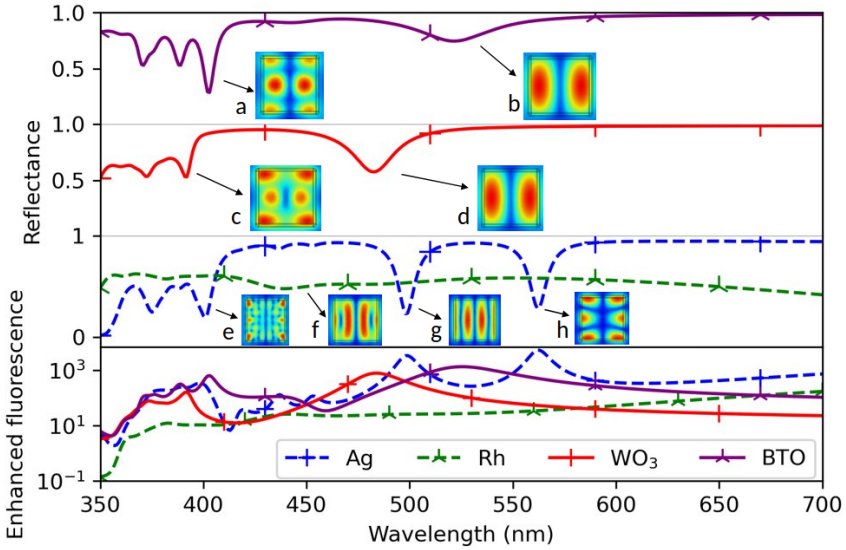

Fig. 2. Reflectance (top three rows) and averaged enhanced fluorescence (bottom row) induced by Ag, Rh, WO_3 and BTO nanocubes (L=150 nm) on a dielectric gap (n=1.54, w=10 nm) and a silver substrate illuminated at normal incidence. The inserts, labelled a to h, show the electric field intensity maps in a (x, y) cross-section in the middle of the dielectric gap and represent the modes at the resonances referred to by the corresponding arrows. The highest intensity, in red, corresponds to the maximum of the norm of the electric field on the represented plane, for each mode independently. The cube edges are represented by the thin black lines in each image. The polarization of the exciting electric field is as represented on the Fig. 1.

We write the fluorescence rate as [51]:

$$\gamma_{em} = \gamma_{exc} \frac{\gamma_r}{\gamma}, \tag{1}$$

with γ_{exc} the excitation rate, γ_r the radiative decay rate and γ the total decay rate. The excitation rate is proportional to the square of the scalar product between the exciting electric field and the normalised dipolar moment of the fluorophore at the fluorophore positions: $\left|\boldsymbol{E_{exc}} \cdot \boldsymbol{n_p}\right|^2$. Therefore, the strong and localized electromagnatic field underneath the nanocube can lead to a significant enhancement of the absorption. The total decay rate can be derived from the dyadic Green function of the system and is proportional to [11,51] $\mathrm{Im}(\boldsymbol{p} \cdot \boldsymbol{E_{sp}})$, with $\boldsymbol{E_{sp}}$ the electric field emitted by a dipole of dipolar moment $\boldsymbol{p}$, measured at the dipole position. Finally, the radiation rate is proportional to the power radiated by the dipole in the direction of a detector, taken at normal incidence with a numerical aperture of 0.9, called P_{ap}.

When comparing the fluorescence rate of a system with nanocube to a system without nanocube and silver substrate, we can simplify all the proportionality factors and write the fluorescence enhancement as:

$$\langle EF \rangle = \frac{\left\langle \left|\boldsymbol{E_{exc}} \cdot \boldsymbol{n_p}\right|^2 \right\rangle}{\left\langle \left|\boldsymbol{E^0_{exc}} \cdot \boldsymbol{n_p}\right|^2 \right\rangle} \frac{\left\langle P_{ap}/\mathrm{Im}(\boldsymbol{p} \cdot \boldsymbol{E_{sp}}) \right\rangle}{\left\langle P^0_{ap}/\mathrm{Im}(\boldsymbol{p} \cdot \boldsymbol{E^0_{sp}}) \right\rangle}, \tag{2}$$

where the superscript 0 denotes the reference configuration without the nanocube and the silver substrate. We average the excitation, radiation and total decay rates over the possible orientations and positions of the fluorophores underneath the nanocubes.

Optics EXPRESS

We compare the averaged fluorescence induced by the nanocubes of silver, rhodium, BTO and WO_3 to the fluorescence of the fluorophores deposited on a glass substrate in the bottom row of Fig. 2. The fluorophores emission is largest at $\lambda = 665$ nm. When the wavelength of the exciting light is tuned, the influence of the resonant modes of the different nanocubes on the fluorescence can be explored.

Silver nanocubes offer the largest enhancement, 5400 (mode h) and 3500 (node g) , while the peak in enhancement for the rhodium nanocube at resonance is barely noticeable at 30 (mode f). Dielectric nanocubes enhance the fluorescence up to a maximum of 800 for WO_3, (mode d), and 1400 for BTO, (mode b). These values, while smaller than for silver, are much larger than for rhodium. We summarise the emission properties of the NPAs considered, $\frac{\gamma_r}{\gamma}$, in Table S1 of Supplement 1, in which we relate the poor enhanced fluorescence induced by the rhodium NPA to the material losses. The enhanced fluorescence at resonance of dielectric nanocubes is comparable to metallic nanocubes across the spectrum. In the near UV the (mode a) of BTO, (mode c) of WO_3 and (mode e) of silver nanocubes respectively enhances the fluorescence by a factor of 650, 150 and 300.

Interestingly, the fluorescence enhancement, while being maximum at resonance, is still significant across the entire spectrum. For example, silver nanocubes induced an increased fluorescence enhancement by a factor of 100 from 470 nm to 700 nm despite having only two resonances in this region with a bandwidth of a few tens of nanometers. This effect is reported in the literature as the consequence of the metallic substrate [11,52].

Finally, as can be seen from the mode profiles in Fig. 2, plasmonic modes of lower order have a better spatial coverage of the volume underneath the nanocube. The enhancement of the absorption of light being proportional to the square of the amplitude of the electric field at the position of the absorber, this can be relevant for experimental work dealing with a low concentration of absorbers.

The computed fluorescence of metallic and hybrid NPAs can be put in perspective with the estimated Purcell factor of more complex setups coupling metallic nanoparticles with dielectric photonic crystal cavities, like those theoretically studied in [33,34]. Those systems designed for an optimised Purcell factor, $F_P = \frac{3Q}{4\pi^2 V_m}$, report quality factors, Q, up to 10^5 with normalised volume modes $V_m = \frac{V}{(\lambda/n)^3}$ down to 10^{-4}. The quality factors of the modes reported in this section range from 10, for the mode f of rhodium, to 60 for the modes a of BTO and c of WO_3. The quality factors for these dielectrics is improved compared to those of silver which range between 30 and 40 for the modes h and e respectively. We can estimate the volume mode to be of the order of magnitude of the volume of the gap underneath the nanocube. At a resonance wavelength $\lambda = 400$ nm and for 150 nm large nanocubes on a 10 nm dielectric of refractive index $n = 1.54$, the normalised volume mode is about 10^{-2}. Although the optimised systems mentioned have a predicted greater Purcell factor than the NPAs, we argue in favour of the simplicity of NPAs, whose experimental realization has been demonstrated as mentioned in the introduction.

2.2. Internal modes

An additional feature of dielectric nanocubes is the existence of electromagnetic modes inside the nanocubes. As light can propagate inside the nanocube, the nanocube volume can act like another Fabry-Perot cavity. Although these modes are significantly different from the plasmonic modes, they have the same reflectance profile leading to an enriched reflectance spectrum.

In Fig. 3 we show the reflectance spectrum of a BTO nanocube, focusing on the region of the spectrum where both a plasmonic mode and an internal mode can be seen. Both modes induce a dip in the reflectance due to the trapping of light into their respective cavities and one can only make the distinction between them by inspecting the electromagnetic profile of the nanocube at resonance.

Optics EXPRESS

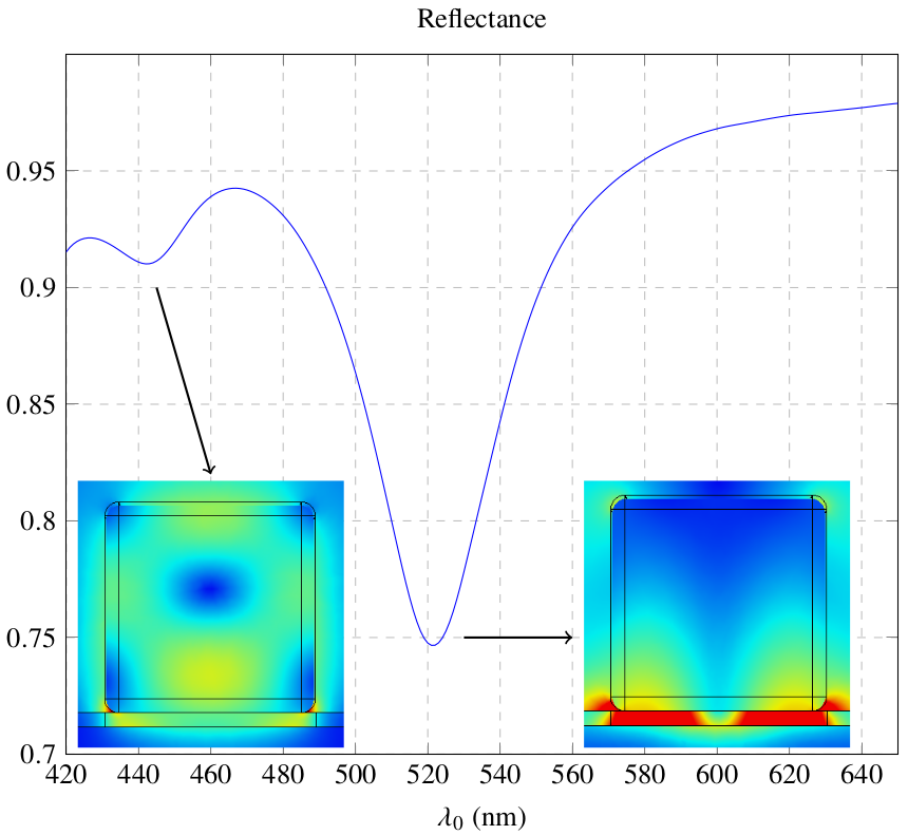

Fig. 3. Reflectance of BTO nanocube (L=150 nm) on a dielectric gap (n = 1.54, w=10 nm) over a silver substrate. Inserted images represent the internal (left) and plasmonic mode (right), (mode b) in Fig. 2. They are colour-coded images of the electric field intensity in a lateral (x, z)-cross-section in the middle of the nanocube and the gap. The highest intensity, in red, corresponds to the norm of the electric field equal to 10 times the norm of the exciting electric field. The cube edges are represented by the thin black lines in each image. The polarization of the exciting electric field is as represented on Fig. 1. The dip in the spectrum due to the internal model is not visible on the scale of the top row of Fig. 2.

Despite the modes being more strongly localised in the nanocube instead than in the gap, internal modes can also slightly enhance the fluorescence by increasing the excitation in the gap, by a factor of 100 for the BTO nanocubes at 440 nm as can be seen on Fig. 2.

2.3. Simplified model of the plasmonic modes

It is possible to use a simple model of the gap plasmonic modes for generic NPA to explain the shift in resonance of BTO or WO_3 nanocubes with respect to siver nanocubes. In this we neglect the internal modes of the nanocubes. This is justified for intermediate refractive index nanocubes as the effect of the internal modes is very small, as shown in Fig. 3.

The abrupt change in refractive index above the dielectric film at the boundaries of the nanocube creates effective mirrors forming a cavity underneath the nanocube. This region, see Fig. 1, acts as a Fabry-Perot cavity whose resonant modes are, therefore, dependent on the optical properties of the nanocube, gap and substrate as well as the dimension of the nanocubes [23].

Optics EXPRESS

To estimate the properties of surface plasmons in a standard or hybrid NPA we compute the electromagnetic modes of three infinitely extended layers corresponding to the substrate, gap material and nanocube. The three layers are characterised by the optical properties of the materials 1 (substrate), 2 (gap) and 3 (nanocube), given by their dielectric permittivity ϵ_1, ϵ_2 and ϵ_3 respectively, and by the thickness w of the gap. We justify the infinitely extended approximation by the large ratio between the size of the nanocube and the thickness of the gap, which is typically between 5 and 30.

In each layer, the magnetic field satisfies the Helmholtz equation [53]:

$$\Delta \boldsymbol{H}_i + k^2 \boldsymbol{H}_i = 0; \qquad k^2 = k_0^2 \epsilon_i; \qquad i = 1, 2, 3; \tag{3}$$

with $\boldsymbol{H}_i$ nand ϵ_i the magnetic field and dielectric permittivity of the layer i respectively and k_0 the wavenumber in vacuum. In the infinitly extend layers approximation, Eqs. (3) can be solved for a magnetic field propagating in the direction tangent to the interfaces and whose component only varies in the direction orthogonal to them. The Eqs. (3) and the boundary conditions of the electromagnetic field at each interface between the layers 1,2 and 3 completly constrain the problem, whose non trivial solutions are the electromagnetic modes of the three infinitely extended layers system. These modes satisfy the following relation, which is a generalization of previous work [54] to a configuration with three different materials instead of two:

$$\tanh(w\alpha_2) + \frac{\alpha_2 \epsilon_2 (\alpha_3 \epsilon_1 + \alpha_1 \epsilon_3)}{\alpha_1 \alpha_3 \epsilon_2^2 + \alpha_2^2 \epsilon_1 \epsilon_3} = 0, \tag{4}$$

where $\alpha_i = \sqrt{k_x^2 - k_0^2 \epsilon_i}$ and k_x is the x-component of the complex wavevector. We numerically solve this equation in terms of the complex number k_x from which we extract the surface plasmon wavelength, $\lambda_{SP} = \frac{2\pi}{\Re(k_x)}$, and propagation length, $\ell_{SP} = \frac{1}{\Im(k_x)}$.

The modes of the NPA are those of a Fabry-Perot cavity of dimension equal to the length of the nanocube [1]. Therefore, the resonant condition can be written as $\frac{2\pi L}{\lambda_{SP}} = n\pi + \phi$, where L is the length of the cube side, $n \in \mathbb{N}$ is the order of the mode and ϕ is the phase change upon reflection, i.e., the argument of the (complex) reflection coefficient. Although we cannot compute the phase reflection coefficient with this approach, we can estimate the wavelength of the resonant modes of order n from knowing the dimension of the nanocube and the surface plasmon wavelength.

The propagation length of the surface plasmons can be used to estimate the strength of the resonant modes. Indeed, if ℓ_{SP} is smaller than the length of the nanocube, strong resonant modes cannot exist as the attenuation of the modes propagating back and forth underneath the nanocube is too pronounced.

We model a NPA by choosing the substrate (material 1), as silver and the gap (material 2), as the PEM typically used to fix the nanocubes of the substrate. The thickness w is taken to be between 6 nm and 20 nm. We use the estimation of the surface plasmon wavelength and propagation length from Eq. (4) to compare different materials for the nanocubes, (material 3). We consider here nanocubes made of a metal, silver, an intermediate refractive index dielectric, BTO, and a fictious nanocube made of a low refractive index (n=1.5) glass.

The propagation length plots in Fig. 4(a) indicates clearly that both dielectric and silver nanocubes NPA could support plasmonic modes as their propagation length is larger than the dimension of the nanocubes. Configurations with a dielectric material 3 have significantly larger propagation lengths due to the absence of electromagnetic losses in their region.

We found a systematic shift in λ_{SP} for dielectrics, compared to silver, as seen in Fig. 4(b). This can be interpreted as a consequence that the configuration with a dielectric material 3 allows a larger presence of the electromagnetic field than if it were a metal. Therefore, its refractive index has a greater influence on the effective refractive index sensed by the cavity modes.

This shift in λ_{SP} implies a systematic blue shift of the dielectric versus silver nanocubes modes. Indeed, if a silver nanocube has a resonant mode at $\lambda_{Ag} = 600$ nm, a BTO nanocube of the same

Optics EXPRESS

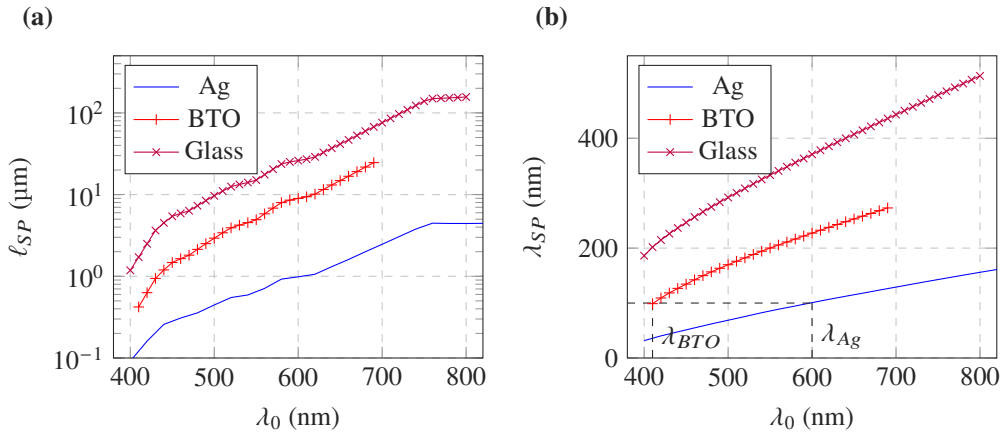

Fig. 4. Surface plasmon propagation length (a) and surface plasmon wavelength (b) as a function of the excitation wavelength for three different nanocubes materials. For all traces the substrate is silver and the gap is a dielectric with refractive index 1.54 and thickness w=6 nm.The vacuum wavelength of a silver/silver or silver/BTO cavity corresponding to a surface plasmon wavelength of 100 nm is identified by λ_{Ag} and λ_{BTO}.

dimension, will have the same resonant mode at approximately 410 nm, Fig. 4(b). The shift in λ_{SP} is found to be inversely proportional to the refractive index of the dielectric considered for the nanocube material. Low refractive index as the glass used in Fig. 4(b) have such a large shift that the plasmonic modes of the hybrid NPA would occur for very short wavelengths. However, a low refractive index dielectric nanocube is expected to have weaker plasmonic resonances. The boundary between the nanocube and the surrounding air forms an effective cavity mirror whose reflectivity is proportional to the difference in refractive index between cube and air. Low refractive index cubes will form cavities with poor mirrors and will, therefore, be unable to support significant resonant effects.

Although this model gives insight in the properties of gap plasmonic modes of generic NPA, and explains the shift in resonance between the modes of BTO and WO_3 compared to silver, it is too simple to assert that any given NPA configuration would have a gap plasmonic mode where it is predicted and it cannot predict internal modes. Numerical simulations of the optical response, like those in section 2.1, are required to confirm the existence and properties of gap plasmonic modes, as well as how well they can couple to exciting light.

2.4. *High refractive index materials*

Hybrid NPA made of high refractive index (n>3) low losses dielectrics have a more complex reflectance spectrum than intermediate refractive index hybrid NPA. We illustrate this in Fig. 5 where we show the spectra and modes of GaP and Si hybrid NPAs.

For intermediate refractive index nanocubes, internal modes were a weak perturbation of the optical spectrum while leaving undisturbed the gap plasmonic modes. For hight refractive index nanocubes, the interaction between the two is stronger and more complex.

As can be seen in the inserts of Fig. 5, the field of a mode is localised both inside the nanocubes and in the gap. This is in contrast with Fig. 3 where the field is predominantly localised either in the nanocube or in the gap, depending on the mode.

This hybridization between the internal and gap plasmonic mode lead to a complexification of the optical spectrum of hybrid NPA made of high refractive index nanocubes. However, the more spatially extended localization of the electromagnetic field reduces both the enhanced excitation

Optics EXPRESS

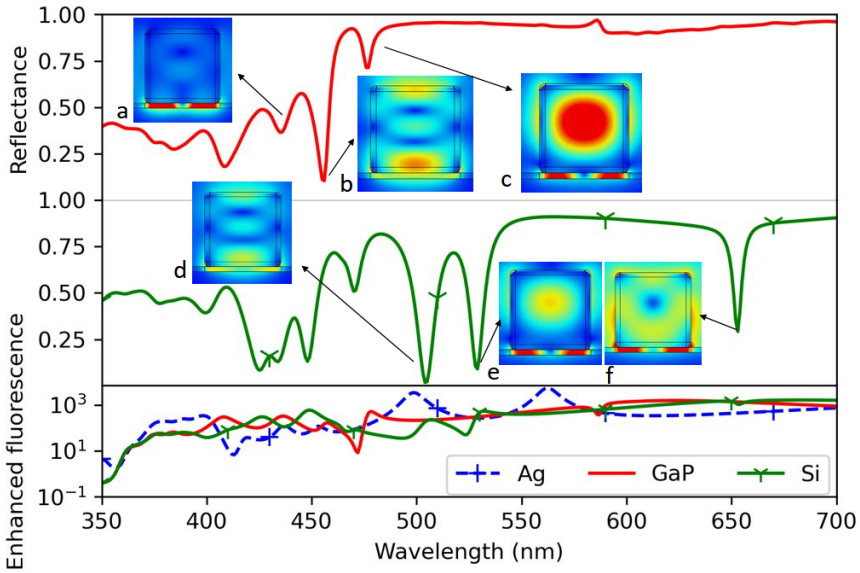

Fig. 5. Reflectance (top two rows) and averaged enhanced fluorescence (bottom row) induced by GaP and Si nanocubes (L=150 nm) on a dielectric gap (n=1.54, w=10 nm) and a silver substrate. The enhanced fluorescence induced by silver nanocubes as in Fig. 2 is added for comparison. The inserts, labelled a to f, show the electric field intensity maps in a (x, z)-cross-section in the middle of the nanocube and the gap, and represent the modes at the resonances referred to by the corresponding arrows. The highest intensity, in red, corresponds to the norm of the electric field equal to 10 times the norm of the exciting electric field. The cube edges are represented by the thin black lines in each image. The polarization of the exciting electric field is as represented on the Fig. 1.

rate at resonance, and the enhanced emission, due to a larger volume mode. Indeed, we can see on the lower panel of Fig. 5 that the fluorescence enhancement at resonance of GaP and Si are relatively weaker than for WO_3 and BTO, Fig. 2, and that silver nanocubes still provides the largest enhancement.

3. Conclusions

Nanopatch antennas are efficient systems for strong light matter interactions in a subwavelength region with applications ranging from sensing to quantum information [55]. We theoretically showed that nanopatch antennas made of high refractive index dielectric nanocubes have an optical spectrum enriched from the hybridization between internal and gap plasmonic modes. Nanopatch antennas made of intermediate refractive index dielectric nanocubes have similar plasmonic modes, optical response and fluorescence enhancement as their metallic counterparts, but blue-shifted. The strong optical properties of hybrid nanopatch antennas made of low-losses dielectric, like those we have studied, make them interesting alternatives to metallic ones for surface enhanced spectroscopy with weaker perturbations induced by Joule heating [31]. Additionally, the significantly shifted resonances, up to 170 nm in the configurations considered in this work, hint a potential extension of the existing applications of metallic nanocubes for shorter wavelength, due to the better spatial coverage of lower order modes. As the fabrication and the characterization of the dielectric nanocubes used in this study have already been reported in the literature, our results offer an important direction and design for practical realization of such systems and their applications.

Optics EXPRESS

4. Methods

The numerical simulations were done using the electromagnetic waves, frequency domain interface of the optics module of the software COMSOL 5.6, solved with a direct solver [56].

Two different sets of simulations were needed to compute first, the reflectance spectrum and the excitation part of the enhanced fluorescence, second, the emission enhancement.

In the first set of simulations, we considered a nanocube with rounded corners (curvature of 10 nm) embedded in a cuboid domain. The bottom and top parts of the integrating domain are Perfectly Matched layers preventing any back reflections. The lateral sides of the domains are encoded with Floquet periodic boundary conditions. We chose, without loss of generality, an exciting light at normal incidence polarised in the $x-$ direction. The reflectance was extracted using ports conditions. To compute the excitation enhancement, we consider a uniform and continuous distribution of the dipole orientations and positions in the dielectric layer under the nanocube. The computation of the electromagnetic profile in this region of the system allows us to directly compute the average of the excitation enhancement, proportional to $\left\langle \left| \boldsymbol{E_{exc}} \cdot \boldsymbol{n_p} \right|^2 \right\rangle$. The lateral size of the domain, equivalent to the periodicity of the nanocubes array, is taken to be 300 nm. Different values for the periodicity can modify the optical response of the overall system, however, this choice of the periodicity still allows for an optical response dominated by those of isolated nanocubes [9].

In the second set of simulations, the geometry of the nanocube is kept the same. However, we considered a large spherical domain with scattering boundary conditions surrounding the nanocube. We computed the emission enhancement of the system, proportional to $P_{ap}/\mathrm{Im}(\boldsymbol{p} \cdot \boldsymbol{E_{sp}})$ for individual dipoles located underneath the nanocube and emitting at λ_{sp} = 665 nm. The radiated power, P_{ap}, is computed by integrating the the far-field flux of energy sent at normal incidence with a numerical aperture of 0.9. The imaginary part of the electric field at the position of the dipole is directly obtained from the computation of the electromagnetic profile in the system. The averaged emission enhancement was computed by varying the position of the dipoles, taken to be located on a 11×11 lattice in the middle of the dielectric substrate. As the radiated power and the enhancement of the spontaneous emission rate are largely dominated by the dipoles with an orientation normal to the surface [11,12], we sped up the computation by only considering this orientation for the dipoles under the nanocubes.

The optical properties of Silver [57], Rhodium [58], GaP [59] (n>3.1) and Si [60] (n>3.6) were provided by the COMSOL material library. The refractive index of the PEM was taken to be 1.54 [23]. We found in the literature the optical properties of WO_3 [46] (n ∈ [1.9, 2.3]) and BTO [61]. We have neglected the birefringence of BTO and modelled it as an isotropic material with refractive index equal to the extraordinary refractive index ($n_e \in [2.3, 2.8]$, Δn<0.1). We used the Sellmeir expansion [61] to extrapolate the optical response of this material for wavelengths shorter than 400 nm.

As mentioned in the introduction, the gap thickness has a strong influence on the optical properties of NPA. We put a quantitative comparison of the reflectance and enhanced fluorescence of silver nanocubes NPA for different gap thickness in section 2 of Supplement 1, for the interested readers.

Funding. Leverhulme Trust (RPG-2019-055).

Acknowledgments. We were introduced to the concept of metallic nanocubes as nanopatch antennas by the work David R. Smith, Alexandre Baron, Stéphane Larouche and Maiken H. Mikkelsen from Duke University during MK's visit. We would like to thank them for the fruitful discussions.

The authors thank Nina Podoliak and Vassilli Fedotov for their constructive feedback during the completion of this project.

The authors acknowledge the use of the IRIDIS High Performance Computing Facility, and associated support services at the University of Southampton, in the completion of this work.

Disclosures. The authors declare no conflicts of interest.

Optics EXPRESS

Data availability. Data underlying the results presented in this paper are not publicly available at this time but may be obtained from the authors upon reasonable request.

Supplemental document. See Supplement 1 for supporting content.

References

1. J. J. Baumberg, J. Aizpurua, M. H. Mikkelsen, and D. R. Smith, "Extreme nanophotonics from ultrathin metallic gaps," Nat. Mater. **18**(7), 668–678 (2019).
2. B. P. Isaacoff and K. A. Brown, "Progress in top-down control of bottom-up assembly," (2017).
3. F. Sterl, E. Herkert, S. Both, T. Weiss, and H. Giessen, "Shaping the color and angular appearance of plasmonic metasurfaces with tailored disorder," ACS Nano **15**(6), 10318–10327 (2021).
4. P. M. Walmsness, N. Hale, and M. Kildemo, "Dispersion of resonant modes in patch antenna lattices," Opt. Lett. **47**(1), 158–161 (2022).
5. A. Klinkova, R. M. Choueiri, and E. Kumacheva, "Self-assembled plasmonic nanostructures," Chem. Soc. Rev. **43**(11), 3976–3991 (2014).
6. A. Yadav, N. Yadav, V. Agrawal, S. P. Polyutov, A. S. Tsipotan, S. V. Karpov, V. V. Slabko, V. S. Yadav, Y. Wu, H. Zheng, and S. RamaKrishna, "State-of-art plasmonic photonic crystals based on self-assembled nanostructures," J. Mater. Chem. C **9**(10), 3368–3383 (2021).
7. J. B. Lassiter, F. McGuire, J. J. Mock, C. Ciracì, R. T. Hill, B. J. Wiley, A. Chilkoti, and D. R. Smith, "Plasmonic waveguide modes of film-coupled metallic nanocubes," Nano Lett. **13**(12), 5866–5872 (2013).
8. Q.-Y. Lin, Z. Li, K. A. Brown, M. N. O'Brien, M. B. Ross, Y. Zhou, S. Butun, P.-C. Chen, G. C. Schatz, V. P. Dravid, K. Aydin, and C. A. Mirkin, "Strong coupling between plasmonic gap modes and photonic lattice modes in dna-assembled gold nanocube arrays," Nano Lett. **15**(7), 4699–4703 (2015).
9. Q. Shen, A. M. Boyce, G. Yang, and M. H. Mikkelsen, "Polarization-controlled nanogap cavity with dual-band and spatially overlapped resonances," ACS Photonics **6**(8), 1916–1921 (2019).
10. R. Faggiani, J. Yang, and P. Lalanne, "Quenching, plasmonic, and radiative decays in nanogap emitting devices," ACS Photonics **2**(12), 1739–1744 (2015).
11. A. Rose, T. B. Hoang, F. McGuire, J. J. Mock, C. Ciracì, D. R. Smith, and M. H. Mikkelsen, "Control of radiative processes using tunable plasmonic nanopatch antennas," Nano Lett. **14**(8), 4797–4802 (2014).
12. G. M. Akselrod, C. Argyropoulos, T. B. Hoang, C. Ciracì, C. Fang, J. Huang, D. R. Smith, and M. H. Mikkelsen, "Probing the mechanisms of large purcell enhancement in plasmonic nanoantennas," Nat. Photonics **8**(11), 835–840 (2014).
13. T. B. Hoang, G. M. Akselrod, and M. H. Mikkelsen, "Ultrafast room-temperature single photon emission from quantum dots coupled to plasmonic nanocavities," Nano Lett. **16**(1), 270–275 (2016).
14. G. M. Akselrod, M. C. Weidman, Y. Li, C. Argyropoulos, W. A. Tisdale, and M. H. Mikkelsen, "Efficient nanosecond photoluminescence from infrared pbs quantum dots coupled to plasmonic nanoantennas," ACS Photonics **3**(10), 1741–1746 (2016).
15. W. M. Wilson, J. W. Stewart, and M. H. Mikkelsen, "Surpassing single line width active tuning with photochromic molecules coupled to plasmonic nanoantennas," Nano Lett. **18**(2), 853–858 (2018).
16. S. I. Bogdanov, M. Y. Shalaginov, A. S. Lagutchev, C.-C. Chiang, D. Shah, A. S. Baburin, I. A. Ryzhikov, I. A. Rodionov, A. V. Kildishev, A. Boltasseva, and V. M. Shalaev, "Ultrabright room-temperature sub-nanosecond emission from single nitrogen-vacancy centers coupled to nanopatch antennas," Nano Lett. **18**(8), 4837–4844 (2018). PMID: 29969274.
17. G. M. Akselrod, T. Ming, C. Argyropoulos, T. B. Hoang, Y. Lin, X. Ling, D. R. Smith, J. Kong, and M. H. Mikkelsen, "Leveraging nanocavity harmonics for control of optical processes in 2d semiconductors," Nano Lett. **15**(5), 3578–3584 (2015).
18. V. Iyer, Y. S. Phang, A. Butler, J. Chen, B. Lerner, C. Argyropoulos, T. Hoang, and B. Lawrie, "Near-field imaging of plasmonic nanopatch antennas with integrated semiconductor quantum dots," APL Photonics **6**(10), 106103 (2021).
19. B. Bahari, R. Tellez-Limon, and B. Kante, "Directive and enhanced spontaneous emission using shifted cubes nanoantenna," J. Appl. Phys. **120**(9), 093106 (2016).
20. S. K. Andersen, S. Kumar, and S. I. Bozhevolnyi, "Ultrabright linearly polarized photon generation from a nitrogen vacancy center in a nanocube dimer antenna," Nano Lett. **17**(6), 3889–3895 (2017).
21. F. Benz, R. Chikkaraddy, A. Salmon, H. Ohadi, B. De Nijs, J. Mertens, C. Carnegie, R. W. Bowman, and J. J. Baumberg, "Sers of individual nanoparticles on a mirror: size does matter, but so does shape," J. Phys. Chem. Lett. **7**(12), 2264–2269 (2016).
22. K. Bedingfield, E. Elliott, N. Kongsuwan, J. J. Baumberg, and A. Demetriadou, "Morphology dependence of nanoparticle-on-mirror geometries: A quasinormal mode analysis," EPJ Appl. Metamat. **9**, 3 (2022).
23. A. Moreau, C. Ciracì, J. J. Mock, R. T. Hill, Q. Wang, B. J. Wiley, A. Chilkoti, and D. R. Smith, "Controlled-reflectance surfaces with film-coupled colloidal nanoantennas," Nature **492**(7427), 86–89 (2012).
24. B. H.-J. Lee and G. Arya, "Orientational phase behavior of polymer-grafted nanocubes," Nanoscale **11**(34), 15939–15957 (2019).
25. X. Zhang, P. Li, Y. Gutiérrez, F. González, F. Moreno, H. O. Everitt, and J. Liu, "Size-tunable rhodium nanostructures for wavelength-tunable ultraviolet plasmonics," Nanoscale Horiz. **1**(1), 75–80 (2016).

Optics EXPRESS

26. Y. Zhang, R. Esteban, R. A. Boto, M. Urbieta, X. Arrieta, C. Shan, S. Li, J. J. Baumberg, and J. Aizpurua, "Addressing molecular optomechanical effects in nanocavity-enhanced raman scattering beyond the single plasmonic mode," Nanoscale **13**(3), 1938–1954 (2021).
27. W. Chen, P. Roelli, H. Hu, S. Verlekar, S. P. Amirtharaj, A. I. Barreda, T. J. Kippenberg, M. Kovylina, E. Verhagen, A. Martínez, and C. Galland, "Continuous-wave frequency upconversion with a molecular optomechanical nanocavity," Science **374**(6572), 1264–1267 (2021).
28. S. Lee, "Nanoparticle-on-mirror cavity: a historical view across nanophotonics and nanochemistry," J. Korean Phys. Soc. **81**(6), 502–509 (2022).
29. J. Huang, A. J. Traverso, G. Yang, and M. H. Mikkelsen, "Real-time tunable strong coupling: from individual nanocavities to metasurfaces," ACS Photonics **6**(4), 838–843 (2019).
30. Y.-L. Kuo, S.-Y. Chuang, S.-Y. Chen, and K.-P. Chen, "Enhancing the interaction between high-refractive index nanoparticles and gold film substrates based on oblique incidence excitation," ACS Omega **1**(4), 613–619 (2016).
31. A. Barreda, J. Saiz, F. González, F. Moreno, and P. Albella, "Recent advances in high refractive index dielectric nanoantennas: Basics and applications," AIP Adv. **9**(4), 040701 (2019).
32. A. Barreda, S. Hell, M. Weissflog, A. Minovich, T. Pertsch, and I. Staude, "Metal, dielectric and hybrid nanoantennas for enhancing the emission of single quantum dots: A comparative study," J. Quant. Spectrosc. Radiat. Transfer **276**, 107900 (2021).
33. A. I. Barreda, M. Zapata-Herrera, I. M. Palstra, L. Mercadé, J. Aizpurua, A. F. Koenderink, and A. Martínez, "Hybrid photonic-plasmonic cavities based on the nanoparticle-on-a-mirror configuration," Photonics Res. **9**(12), 2398–2419 (2021).
34. A. Barreda, L. Mercadé, M. Zapata-Herrera, J. Aizpurua, and A. Martínez, "Hybrid photonic-plasmonic cavity design for very large purcell factors at telecommunication wavelengths," Phys. Rev. Appl. **18**(4), 044066 (2022).
35. Á. Barreda, F. Vitale, A. E. Minovich, C. Ronning, and I. Staude, "Applications of hybrid metal-dielectric nanostructures: State of the art," Adv. Photonics Res. **3**, 2100286 (2022).
36. J. Sautter, I. Staude, M. Decker, E. Rusak, D. N. Neshev, I. Brener, and Y. S. Kivshar, "Active tuning of all-dielectric metasurfaces," ACS Nano **9**(4), 4308–4315 (2015).
37. A. Komar, Z. Fang, J. Bohn, J. Sautter, M. Decker, A. Miroshnichenko, T. Pertsch, I. Brener, Y. S. Kivshar, I. Staude, and D. N. Neshev, "Electrically tunable all-dielectric optical metasurfaces based on liquid crystals," Appl. Phys. Lett. **110**(7), 071109 (2017).
38. H. Sugimoto and M. Fujii, "Broadband dielectric–metal hybrid nanoantenna: Silicon nanoparticle on a mirror," ACS Photonics **5**(5), 1986–1993 (2018).
39. Y. Yang, O. D. Miller, T. Christensen, J. D. Joannopoulos, and M. Soljacic, "Low-loss plasmonic dielectric nanoresonators," Nano Lett. **17**(5), 3238–3245 (2017).
40. P. Liu, Y. Cao, H. Cui, X. Chen, and G. Yang, "Micro-and nanocubes of silicon with zinc-blende structure," Chem. Mater. **20**(2), 494–502 (2008).
41. B. Tilmann, G. Grinblat, R. Berté, M. Özcan, V. F. Kunzelmann, B. Nickel, I. D. Sharp, E. Cortés, S. A. Maier, and Y. Li, "Nanostructured amorphous gallium phosphide on silica for nonlinear and ultrafast nanophotonics," Nanoscale Horiz. **5**(11), 1500–1508 (2020).
42. N. N. Hasbullah, S. K. Chen, K. B. Tan, Z. A. Talib, J. Y. C. Liew, and O. J. Lee, "Photoluminescence activity of batio3 nanocubes via facile hydrothermal synthesis," J. Mater. Sci.: Mater. Electron. **30**(5), 5149–5157 (2019).
43. K. Kato, F. Dang, K.-I. Mimura, Y. Kinemuchi, H. Imai, S. Wada, M. Osada, H. Haneda, and M. Kuwabara, "Nano-sized cube-shaped single crystalline oxides and their potentials; composition, assembly and functions," Adv. Powder Technol. **25**(5), 1401–1414 (2014).
44. L. Wang, H. Hu, J. Xu, S. Zhu, A. Ding, and C. Deng, "Wo3 nanocubes: Hydrothermal synthesis, growth mechanism, and photocatalytic performance," J. Mater. Res. **34**(17), 2955–2963 (2019).
45. T. Üstün, V. Eskizeybek, and A. Ahmet, "Selectively nanocubes formation of tungsten oxide (wo3)," Celal Bayar Univ. J. Sci. **16**, 149–153 (2020).
46. K. Von Rottkay, M. Rubin, and S.-J. Wen, "Optical indices of electrochromic tungsten oxide," Thin Solid Films **306**(1), 10–16 (1997).
47. I. M. Palstra, H. M. Doeleman, and A. F. Koenderink, "Hybrid cavity-antenna systems for quantum optics outside the cryostat?" Nanophotonics **8**(9), 1513–1531 (2019).
48. K. G. Cognée, H. M. Doeleman, P. Lalanne, and A. Koenderink, "Cooperative interactions between nano-antennas in a high-q cavity for unidirectional light sources," Light: Sci. Appl. **8**(1), 115 (2019).
49. H. M. Doeleman, C. D. Dieleman, C. Mennes, B. Ehrler, and A. F. Koenderink, "Observation of cooperative purcell enhancements in antenna–cavity hybrids," ACS Nano **14**(9), 12027–12036 (2020).
50. I. Shlesinger, I. M. Palstra, and A. F. Koenderink, "Integrated sideband-resolved sers with a dimer on a nanobeam hybrid," Phys. Rev. Lett. **130**(1), 016901 (2023).
51. P. Anger, P. Bharadwaj, and L. Novotny, "Enhancement and quenching of single-molecule fluorescence," Phys. Rev. Lett. **96**(11), 113002 (2006).
52. T. B. Hoang, G. M. Akselrod, C. Argyropoulos, J. Huang, D. R. Smith, and M. H. Mikkelsen, "Ultrafast spontaneous emission source using plasmonic nanoantennas," Nat. Commun. **6**(1), 7788 (2015).
53. L. Novotny and B. Hecht, *Principles of nano-optics* (Cambridge university press, 2012).

Optics EXPRESS

54. S. I. Bozhevolnyi and T. Søndergaard, "General properties of slow-plasmon resonant nanostructures: nano-antennas and resonators," Opt. Express **15**(17), 10869–10877 (2007).
55. H. J. Kimble, "The quantum internet," Nature **453**(7198), 1023–1030 (2008).
56. "Comsol® v. 5.6. www.comsol.com. comsol ab, stockholm, sweden,".
57. K. M. McPeak, S. V. Jayanti, S. J. Kress, S. Meyer, S. Iotti, A. Rossinelli, and D. J. Norris, "Plasmonic films can easily be better: rules and recipes," ACS Photonics **2**(3), 326–333 (2015).
58. J. Weaver, C. Olson, and D. W. Lynch, "Optical investigation of the electronic structure of bulk rh and ir," Phys. Rev. B **15**(8), 4115 (1977).
59. G. Jellison Jr, "Optical functions of gaas, gap, and ge determined by two-channel polarization modulation ellipsometry," Opt. Mater. **1**(3), 151–160 (1992).
60. M. A. Green, "Self-consistent optical parameters of intrinsic silicon at 300 k including temperature coefficients," Solar Energy Materials and Solar Cells **92**(11), 1305–1310 (2008).
61. S. Wemple, M. Didomenico Jr, and I. Camlibel, "Dielectric and optical properties of melt-grown batio3," J. Phys. Chem. Solids **29**(10), 1797–1803 (1968).